

UCSF

UC San Francisco Previously Published Works

Title

convertibleCARs: A chimeric antigen receptor system for flexible control of activity and antigen targeting

Permalink

<https://escholarship.org/uc/item/2cd0685z>

Journal

Communications Biology, 3(1)

ISSN

2399-3642

Authors

Landgraf, Kyle E
Williams, Steven R
Steiger, Daniel
et al.

Publication Date


2020

DOI

10.1038/s42003-020-1021-2

Peer reviewed

*convertible*CARs: A chimeric antigen receptor system for flexible control of activity and antigen targeting

Kyle E. Landgraf¹, Steven R. Williams², Daniel Steiger³, Dana Gebhart², Stephen Lok⁴, David W. Martin², Kole T. Roybal⁵ & Kaman Chan Kim²  ²✉

We have developed a chimeric antigen receptor (CAR) platform that functions as a modular system to address limitations of traditional CAR therapies. An inert form of the human NKG2D extracellular domain (iNKG2D) was engineered as the ectodomain of the CAR to generate *convertible*CARTM-T cells. These cells were specifically directed to kill antigen-expressing target cells only in the presence of an activating bispecific adapter comprised of an iNKG2D-exclusive ULBP2-based ligand fused to an antigen-targeting antibody (MicAbodyTM). Efficacy against Raji tumors in NSG mice was dependent upon doses of both a rituximab-based MicAbody and *convertible*CAR-T cells. We have also demonstrated that the exclusive ligand-receptor partnering enabled the targeted delivery of a mutant form of IL-2 to selectively promote the expansion of *convertible*CAR-T cells in vitro and in vivo. By altering the Fv domains of the MicAbody or the payload fused to the orthogonal ligand, *convertible*CAR-T cells can be readily targeted or regulated.

¹ Reflexion Pharmaceuticals, 937 Tahoe Blvd, Suite 150, Incline Village, NV 89451, USA. ² Xyphos Biosciences, an Astellas Company, 100 Kimball Way, South San Francisco, CA 94080, USA. ³ Freenome, 279 E Grand Ave 5th Floor, South San Francisco, CA 94080, USA. ⁴ Zymergen, 5980 Horton St #105, Emeryville, CA 94608, USA. ⁵ University of California, San Francisco, 513 Parnassus Avenue HSE-301, San Francisco, CA 94143, USA. ✉email: kaman@xyphosinc.com

The engineering of patient-derived T cells to express chimeric antigen receptors (CARs) has altered the landscape of adoptive cell therapies, providing scientists and clinicians the ability to harness the powerful cytolytic capabilities of T cells and direct them to specific antigen-expressing targets in an MHC-independent manner. Their initial application to treat hematologic malignancies has led to astounding responses and inspired a surge of research efforts to improve upon the original designs in order to strike the best balance of CAR-T cell potency, safety, and persistence and to drive their effective use in non-hematologic indications^{1,2}. Sufficient pre-clinical and clinical data have accumulated from the variations on prototype CAR architecture such that there is now a deeper appreciation of the subtleties that affect CAR-T function. However, CAR-T cell therapies are limited by their utilization of a single-purpose targeting domain, lack of dose control which can contribute to cytokine release syndrome, inability to address tumor antigen loss leading to disease relapse, and immunogenicity of non-human targeting domains leading to lack of persistence^{3–5}. There is a need to develop a human-derived modular CAR-T cell system that enables sequential and multiplex targeting and that, ideally, would provide elements of dose controlled activity, expansion, and persistence. A number of creative solutions have been explored utilizing adapter molecules that can engage a constant CAR for differential antigen targeting (reviewed in ref. 6). However, there is no single bio-orthogonal human system that has been demonstrated to have the potential for all the following: flexible targeting to direct T cell activity to antigen of choice, multiplex capabilities to reduce the potential for antigen-loss related relapse, dose control for differential engagement of CAR-T cells, and selective delivery of modulatory agents to CAR-expressing cells.

NKG2D is an activating receptor expressed as a type II homodimeric integral membrane protein on natural killer (NK) cells, some myeloid cells, and certain T cells^{7–9}. Human NKG2D has eight distinct natural MIC ligands (MICA, MICB, ULBP1 through ULBP6) that are upregulated on the surface of cells in response to a variety of stresses and their differential regulation provides the immune system a means of responding to a broad range of emergency cues with minimal collateral damage^{10–12}. The structure of the NKG2D ectodomain, several soluble ligands, and the bound complex of ligands to the ectodomain have been solved, revealing a saddle-like groove in the homodimer interface which engages the structurally conserved $\alpha_1\alpha_2$ domains of the ligands that are otherwise of disparate amino acid identity^{13–16}. Based upon this structure-function information, we have mutated the NKG2D ectodomain to render it incapable of engaging any natural ligands¹⁷. Orthogonal ULBP2 $\alpha_1\alpha_2$ domain ligand variants were then selected to exclusively engage the inert NKG2D (iNKG2D) but not wild-type NKG2D (wtNKG2D). iNKG2D serves as the extracellular component of our CAR construct while the orthogonal ULBP2-S3 variant (U2S3) is expressed as a fusion to antigen-specific antibodies, generating bispecifics termed MicAbodies. MicAbodies are capable of directing and activating iNKG2D-CAR-expressing T cells only when the appropriate antigen is displayed on a surface. Keeping the iNKG2D-CAR receptor constant, we have demonstrated that with either single or multiplexed MicAbodies, *convertible*CAR-T cells can be targeted to different tumor antigens to mediate cytotoxicity. In a disseminated in vivo Raji tumor model, efficacy required both iNKG2D-CAR T cells and MicAbody, both in a dose-dependent manner. Lastly, we have determined that U2S3 can be used as a means of addressing molecules for delivery to iNKG2D-expressing cells and that this feature can specifically target the iNKG2D-CAR cells for complement-mediated killing or drive their expansion in vitro and in vivo with a mutant cytokine

fusion. This highly modular *convertible*CAR system leverages the body of information behind antibody discovery, development, and manufacturing and nimbly integrates it with the tremendous potential of adoptive cell therapies.

Results

Engineering an orthogonal NKG2D-ligand interaction. Two central tyrosine residues in each NKG2D monomer have critical roles in driving receptor-ligand interactions¹⁷ (Fig. 1a). Mutations at these residues were heavily explored, with the Y152A mutant (“iNKG2D.YA”) and the Y152A/Y199F double mutant (“iNKG2D.AF”) selected for further study and confirmed by biolayer interferometry (BLI) (Supplementary Figs. 1a, 3a) and ELISA (Supplementary Fig. 1b) to have lost binding to all naturally occurring human ligands. The ULBP2 $\alpha_1\alpha_2$ domain was chosen for phage display-based selection of mutants with high affinity binding to each of the iNKG2D variants since it is not polymorphic¹⁸. NNK libraries interrogating helix 2 and helix 4 (Fig. 1b, c)¹⁵ returned only helix 4 variants and even then only in the context of a spontaneous R81W mutation which likely has a stabilizing role on the ULBP2 $\alpha_1\alpha_2$ domain. Competitive selection with rounds of increasing concentration of wtNKG2D (Supplementary Fig. 2a) yielded three variants—U2S1, U2S2, and U2S3—that reproducibly bound exclusively to iNKG2D.YA even when reformatted as fusions to the C-terminus of the IgG1 heavy chain of the anti-FGFR3 antibody clone R3Mab (Supplementary Fig. 2b). Although the R81W mutation alone enhanced affinity toward both wtNKG2D and iNKG2D.YA (Supplementary Fig. 2b, c), its presence in the iNKG2D-selective variants was deemed essential since its reversion to the wild-type residue resulted in loss of binding to iNKG2D.YA. As U2S3 consistently exhibited a greater binding differential, it was characterized more thoroughly and shown as a monomer to have a 10-fold higher affinity toward iNKG2D.YA than wild-type ULBP2 had to wtNKG2D (Supplementary Fig. 2c). Picomolar binding to iNKG2D.YA was measured with a bivalent rituximab antibody fusion and orthogonality was retained by both light-chain (LC) and heavy-chain (HC) fusion configurations (Fig. 1d).

Candidate orthogonal variants were similarly identified for iNKG2D.AF and ELISAs comparing rituximab-LC fusions to Fc-wtNKG2D, Fc-iNKG2D.YA, and Fc-iNKG2D.AF identified four variants that selectively bound only iNKG2D.AF (Supplementary Fig. 3b) with the U2R variant being the most selective. ELISAs comparing binding of Rituximab.LC-U2S3 and Rituximab.LC-U2R to both iNKG2D.YA and iNKG2D.AF confirmed that these two independently selected orthogonal ligands exclusively engaged the inert NKG2D variant for which it was evolved (Supplementary Fig. 3c).

Expression of iNKG2D.YA as a chimeric antigen receptor.

Lentiviral transduction of iNKG2D.YA fused to 4-1BB, CD3 ζ , and eGFP into primary human T cells efficiently generated *convertible*CAR-T cells with robust transgene expression on par with a rituximab-scFv based CAR construct (RITscFv-CAR) with the same hinge, transmembrane, and intracellular architecture (Fig. 2b and Supplementary Fig. 4). Surface staining of iNKG2D.YA with the Rituximab.LC-U2S3 MicAbody correlated strongly with GFP expression, suggesting a direct relationship between efficiency of CAR expression and presentation of iNKG2D on the T cell surface (Fig. 2c). Using flow cytometry of Alexa Fluor 647 conjugated Rituximab.LC-U2S3 MicAbody and standard quantification beads, the median amount of iNKG2D.YA expressed on the surface was estimated to be 21,000 molecules. Direct engagement of iNKG2D.YA-CAR receptors by incubation of *convertible*CAR-CD8⁺ cells to microtiter plates coated with wild-type or U2S3 ligands resulted in activation and liberation of IL-2

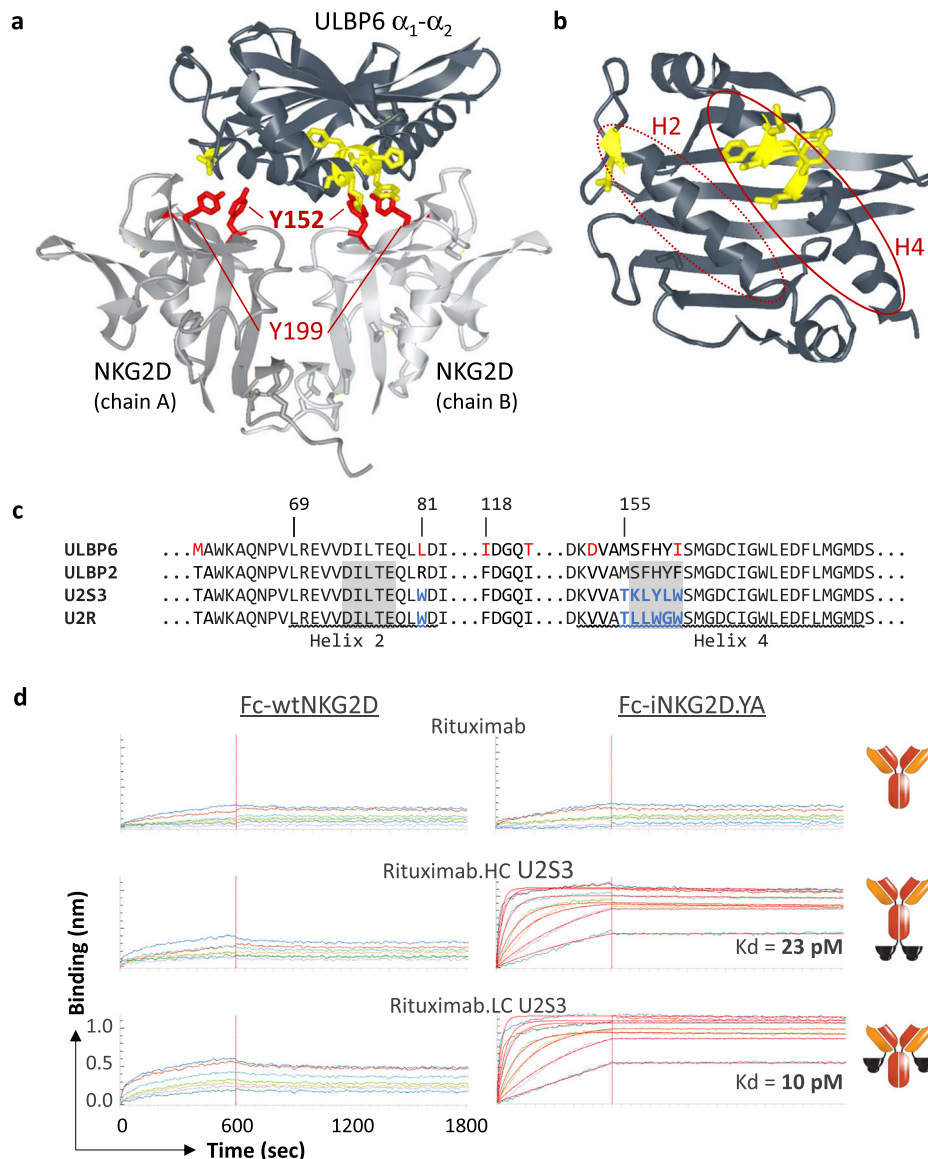


Fig. 1 Structure-based engineering for a novel orthogonal interaction. **a** The structure of NKG2D in complex with ULBP6 (PDB: 450U) was used to illustrate the residues in both the NKG2D homodimer and ligand that were targeted for mutagenesis. Light gray chains correspond to the two NKG2D monomers with Tyrosine 152 and Tyrosine 199, important for ligand engagement, highlighted in red. The dark gray chain corresponds to ULBP6 with the locations of residues 81 and 156–160, mutated in the orthogonal ligands, highlighted in yellow. PDB files were manipulated using the NCBI iCn3D 3D Structure Viewer (<https://www.ncbi.nlm.nih.gov/Structure/icn3d/full.html>). **b** The same ULBP6 structure but with NKG2D absent and the ligand rotated 90° to reveal the two critical helix domains—H2 and H4 (in red ovals)—that engage with the NKG2D homodimer. **c** The ULBP2 and ULBP6 $\alpha_1\alpha_2$ domains are 96.7% identical with the differences in red font. The locations of helices 2 and 4 are underlined, the NNK library residues highlighted in gray, and the residues incorporated into the final orthogonal ligands—ULBP2.S3 (U2S3) and ULBP2.R (U2R) for iNKG2D.YA and iNKG2D.AF, respectively—indicated in blue. Numbering is based upon the mature protein. **d** Octet BLI verification of U2S3 orthogonality when fused to the C-terminus of either the heavy or light chain of rituximab. Fc-wtNKG2D or Fc-iNKG2D.YA were captured with anti-human IgG Fc capture (AHC) biosensor tips then associated with a two-fold dilution series of MicAbody starting at 50 nM. The y-axes corresponding to binding responses were set to the same scale for all sensograms. Kd values could only be calculated for the two positive binding interactions and are shown.

and IFN γ only with U2S3 while wtNKG2D-CAR bearing cells responded only to wild-type ligands confirming the selectivity of the orthogonal interaction in the context of T cells (Supplementary Fig. 5a). Furthermore, activation of *convertible*CAR-T cell function was dependent upon the presence of the appropriate cognate ULBP2 variant. The iNKG2D.YA expressing or iNKG2D.AF expressing T cells only lysed Ramos (CD20⁺) target cells when armed with a MicAbody bearing its respective orthogonal ligand, i.e. U2S3 or U2R (Supplementary Fig. 3d). Co-culture of

Ramos cells alone was not sufficient to drive activation of *convertible*CAR-CD8⁺ cells. Instead the appropriate antigen-targeting MicAbody was required since neither rituximab antibody nor Trastuzumab.LC-U2S3 activated CAR cells whereas Rituximab.LC-U2S3 triggered maximum cytokine release in the 32–160 pM range. Additionally, cytokine release by *convertible*CAR-T cells with Rituximab.LC-U2S3 MicAbody exceeded that of the RITscFv-CAR cells (Supplementary Fig. 5b). These data demonstrated that the appropriate antigen-targeting MicAbody was

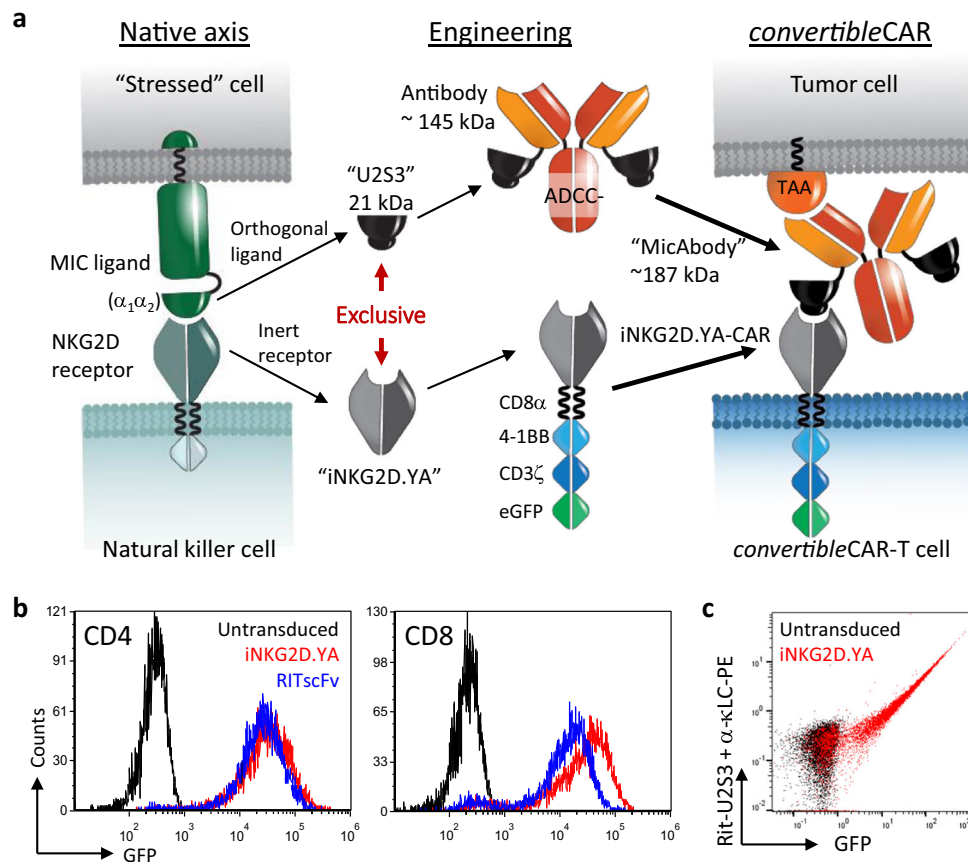


Fig. 2 Elements of the *convertibleCAR* system. **a** Engineering overview to convert components of the NKG2D-MIC axis into the *convertibleCAR* system. iNKG2D.YA and U2S3 became the components of a second generation CAR receptor and bispecific adapter molecule (MicAbody), respectively. “TAA” is tumor-associated antigen. **b** Representative example of high efficiency lentiviral transduction of the iNKG2D.YA-CAR into either CD4 or CD8 cells. Transduction efficiency varied between donors but >70% GFP⁺ yields were consistently achieved. The RITscFv-CAR is shown for comparison and has the same architecture as the iNKG2D-CAR except that an scFv based upon the V_H/V_L domains of rituximab was used instead of iNKG2D.YA. **c** Surface expression of iNKG2D.YA-CAR was determined in CD8⁺ T cells by incubating cells with Rituximab.LC-U2S3 MicAbody followed by PE-conjugated mouse-anti-human kappa chain antibody staining. Untransduced T cells are shown for comparison.

required to form a junction, likely similar to that characterized for scFv-CARs¹⁹, between the target and *convertibleCAR*-T cells to drive robust activation of T cell function (Fig. 3a).

Staining of *convertibleCAR*-CD8⁺ cells with a fluorescently labeled Rituximab.LC-U2S3 MicAbody revealed saturation of total iNKG2D.YA-CAR receptors at 5 nM (Fig. 3b). However, in a co-culture killing experiment where *convertibleCAR*-CD8⁺ cells were armed with decreasing amounts of Rituximab.LC-U2S3, Ramos target cell lysis activity reached a saturation response at 30 pM, two orders of magnitude less than required for full occupancy of receptors (Fig. 3c). This result suggests the extra unoccupied iNKG2D.YA-CAR receptors could be armed with heterologous MicAbodies to guide activity against multiple targets simultaneously. To directly test this, *convertibleCAR*-CD8⁺ cells were armed with Rituximab.LC-U2S3, Trastuzumab.LC-U2S3 (targeting Her2), or an equimolar mixture of the two MicAbodies and exposed to either Ramos cells or CT26-Her2. Although CAR cells armed with a single MicAbody directed lysis to only tumor cells expressing the cognate antigen, dual-armed CARs targeted both tumor cell lines without any compromise in lytic potency (Fig. 3d).

convertibleCAR-T cells inhibit disseminated B-cell lymphomas.

The pharmacokinetics of both the HC and LC Rituximab-U2S3 MicAbodies (Supplementary Fig. 6a) in NSG mice revealed a

β -phase that paralleled the parental antibody with the steeper α -phase of the MicAbodies attributed to retention of U2S3 binding to endogenous mouse wild-type NKG2D (Supplementary Fig. 6c). The LC-U2S3 fusion had a slightly longer terminal half-life than the HC-fused MicAbody, out-performed the HC fusion in an in vitro killing assay with Ramos target cells (Supplementary Fig. 6b), and appeared to be more efficacious at early time points in suppressing Raji B cell lymphoma expansion in NSG mice (Supplementary Fig. 6d, e). Accordingly, Rituximab.LC-U2S3 (Rit-S3) was deployed in further experiments exploring dosing parameters for lymphoma control (Supplementary Fig. 7). An intermediate Rit-S3 dose of 20 μ g was shown to be the most efficacious as high concentrations may result in over saturation of receptors on the CAR cells and antigens on the tumor cells, thereby interfering with productive engagement. Additionally, a higher frequency of Rit-S3 administration of every 2 days versus every 4 days paired with a higher dose (10×10^6) of *convertibleCAR*-T cells resulted in the greatest suppression of tumor growth. Rit-S3 alone was ineffective at tumor control while a graft-vs-tumor effect was consistently observed in both untransduced and *convertibleCAR* only cohorts (Supplementary Fig. 7a, b; Fig. 4b). Rit-S3 was detectable in the serum of mice throughout the course of the study with peak levels appearing earlier with more frequent dosing (Supplementary Fig. 7b).

A Raji disseminated lymphoma model with optimized *convertibleCAR*-T dosing was performed with 20 μ g Rit-S3 dosing every

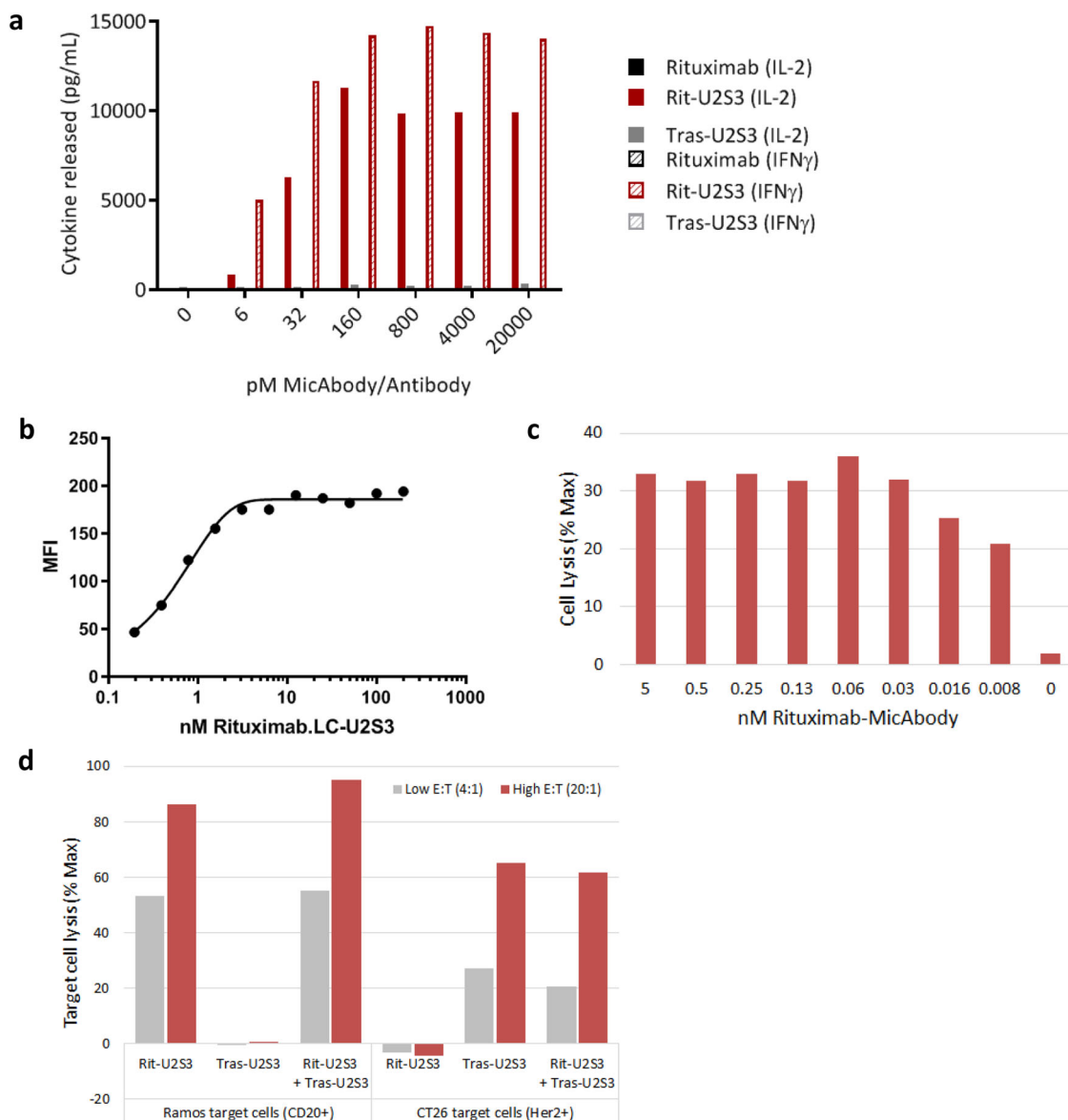


Fig. 3 In vitro characterization of convertibleCAR activity. **a** Ramos (CD20⁺) target cells were exposed to convertibleCAR-CD8⁺ cells at an E:T of 5:1 and co-cultured with increasing concentrations of rituximab antibody (ADCC-deficient), Rituximab.LC-U2S3 MicAbody, or Trastuzumab.LC-U2S3 MicAbody. After 24 h, supernatants were harvested and IL-2 (solid bars) or IFN γ (hatched bars) quantified by ELISA. **b** convertibleCAR-CD8⁺ cells were incubated with increasing concentrations of Alexa Fluor 647 conjugated Rituximab.LC-U2S3 for 30 min, the excess washed away, and the MFI quantified by flow cytometry. Red line at 5 nM indicates inflection point at which receptors are maximally occupied. **c** convertibleCAR-CD8⁺ cells were armed with increasing concentrations of Rituximab.LC-U2S3 as described in (b) then co-incubated with calcein-loaded Ramos cells at an E:T of 20:1 for 2 h after which the amount of released calcein was quantified. **d** iNKG2D.YA-CAR CD8⁺ cells were pre-armed with 5 nM Rituximab.LC-U2S3, 5 nM Trastuzumab.LC-U2S3, or an equimolar mixture of 2.5 nM of each as described in (b) then exposed to calcein-loaded Ramos or CT26-Her2 cells at two indicated E:T ratios. The amount of calcein released was quantified after two hours. Except for b, data are representative of at least two independent experiments and plotted as an average of technical triplicates.

2 days comparing 5×10^6 (5M) to 15×10^6 (15M) convertibleCAR-T cells (Fig. 4a). As a positive control, RITscFv-CAR cells were also included which have in vitro Ramos killing potency comparable to convertibleCAR-T cells (Supplementary Fig. 5b). At 5M total T cells, both RITscFv-CAR and convertibleCARs + Rit-S3 were effective at controlling tumor (Fig. 4b). Although the average tumor bioluminescence signal was lower for the RITscFv-CAR cohort (Fig. 4c), and four of five mice in that cohort appeared to have cleared tumor tissue, three of five mice in the convertibleCAR + Rit-S3 cohort appeared cleared (Fig. 4d). When total infused CAR-T cell doses were increased to 15M cells, both

RITscFv-CAR and convertibleCAR + Rit-S3 were able to completely block tumor expansion (Fig. 4b, d). In all studies, peak levels of peripheral human CD3⁺ T cells consistently appeared around 7 days post-infusion with both scFv-CAR and convertibleCAR-T cells having contracted in the majority of mice by 14 days (Fig. 4f). There was a delayed expansion of CD3⁺ cells in the untransduced and convertibleCAR-only cohorts that was contemporary with the onset of the graft-versus-tumor response and likely the consequence of expansion of specific reactive clones. MicAbody associated convertibleCAR-T cells were observed in the blood of mice in convertibleCAR + Rit-S3 cohorts (Fig. 4g).

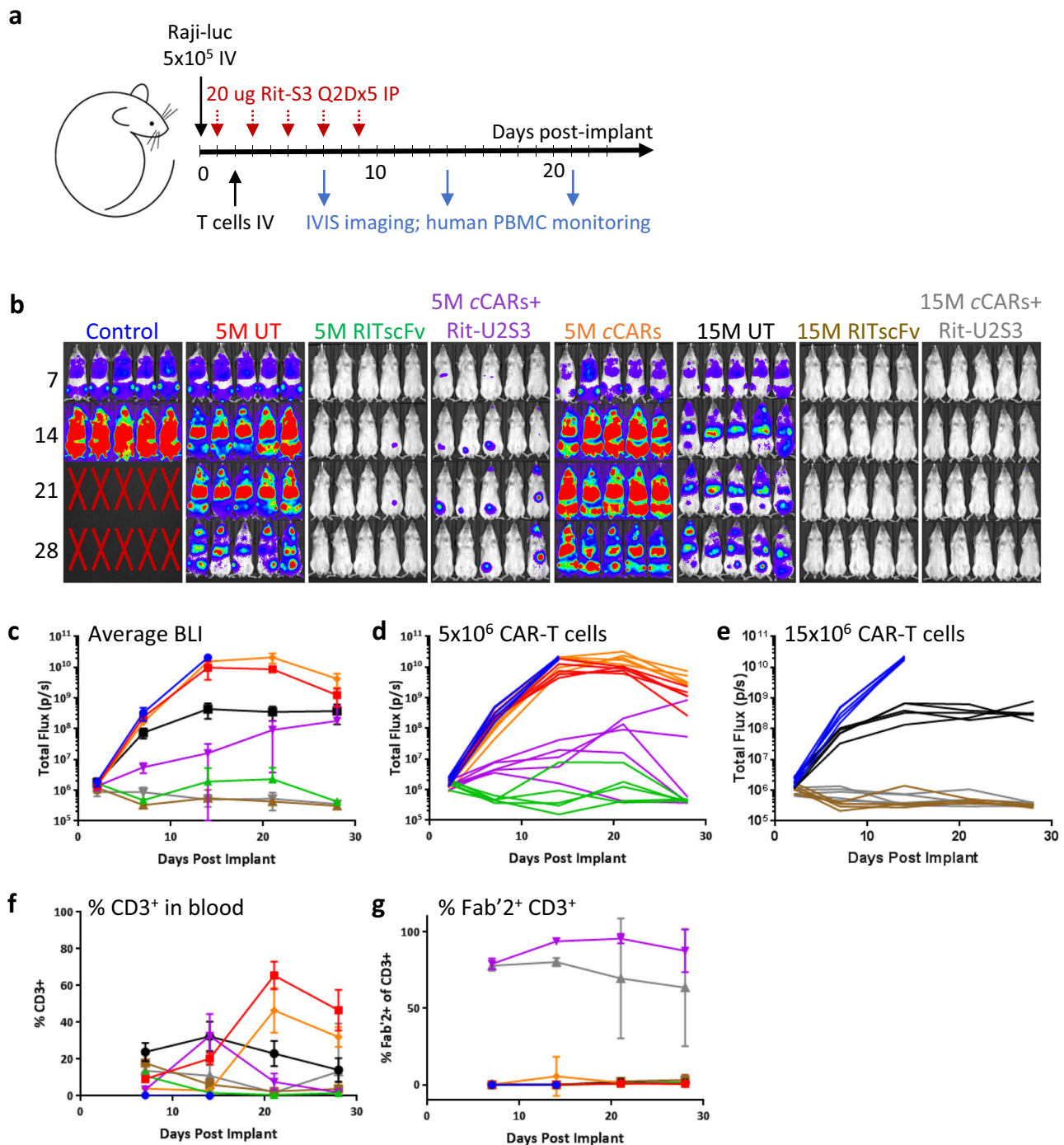


Fig. 4 Control of a disseminated Raji B cell lymphoma in NSG mice. **a** Study design in NSG mice with Raji-luciferase cells implanted IV followed by treatment and monitoring as indicated. **b** IVIS imaging was performed 7, 14, 21, and 28 days post-implantation and all adjusted to the same scale. **c** Average luminescent output \pm SD for each cohort along with individual animal traces for the groups that received **d** 5×10^6 or **e** 15×10^6 total T cells. T cell dynamics over the course of the study examining **f** human CD3⁺ cells in the blood and **g** bound MicAbody detected by anti-F(ab')₂. Shown are cohort averages \pm SD, $n = 5$. Color coding in all graphs matches the labeling on the luminescence images.

convertibleCAR-T cells inhibit subcutaneous lymphomas. Raji B cells were implanted subcutaneously to assess the ability of the *convertibleCAR* system to suppress growth of a solid tumor mass. Once tumors were established at 10 days, either 7×10^6 (7M) or 35×10^6 (35M) *convertibleCAR*-Ts were administered after a single IV dose of 60 μ g Rit-S3 (Fig. 5a). Additionally, one cohort received 35M cells that were pre-armed with a saturating concentration of Rit-S3 cells prior to administration but no additional MicAbody introduced injections. Administration of 7M *convertibleCAR*-T cells

along with Rit-S3 (7M + Rit-S3) resulted in reduced tumor size relative to *convertibleCAR*-T cells alone (Fig. 5b, c). Furthermore, in the 35M + Rit-S3 cohort, tumor growth was completely suppressed. Tumor growth in the cohort that received 35M pre-armed cells was also inhibited. By 2 days post-infusion, *convertibleCAR*-T cells that had been pre-armed did not have detectable surface associated Rit-S3 MicAbody (Fig. 5e), a result of disarming likely due to a combination of activation-induced cell proliferation and the turnover of armed receptors. Serum levels of Rit-S3 were comparable at both

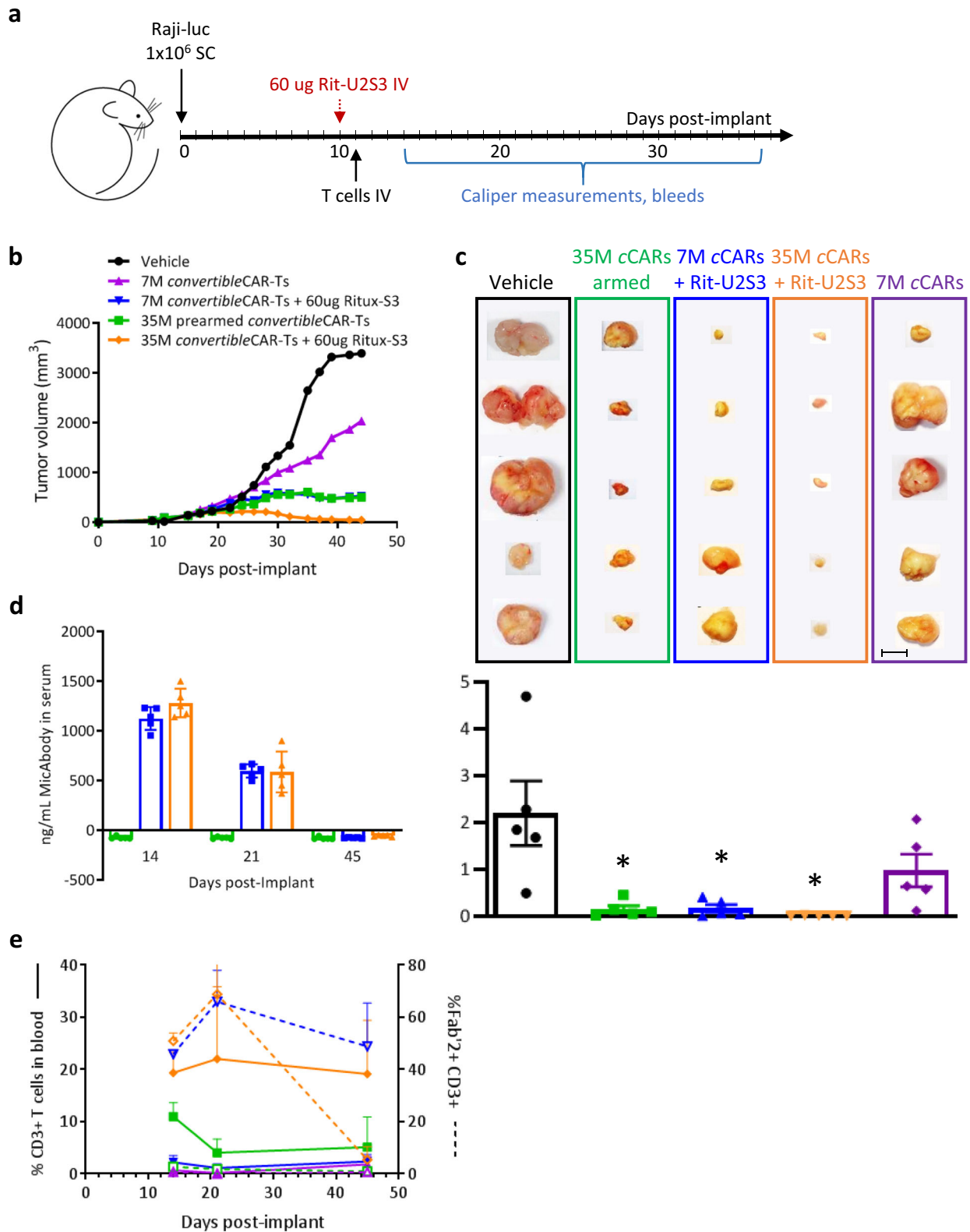


Fig. 5 Control of subcutaneously implanted Raji tumors in NSG mice by convertibleCAR-T cells. **a** Schematic of study design with treatment initiated at day 10 with Rit-S3 administration followed by CAR-T infusion the next day. **b** Average tumor volumes for each cohort, $n = 5$. Tumors varied greatly in size within each group so error bars were not graphed. Two cohorts, blue and green lines, overlap and cannot be graphically distinguished beyond day 26. **c** Excised tumors at day 45 post-implantation with average tumor masses plotted in grams for each cohort, \pm SEM, and * indicating $p < 0.05$ compared to the vehicle cohort as determined by unpaired, two-tailed t -test. Scale bar = 1 cm and all images adjusted to the same scale. **d** Serum Rit-S3 levels. Error bars indicated \pm SD samples from mice in a given cohort. **e** CD3⁺ T cell dynamics in the blood and quantitation of the percentage of T cells with surface-associated MicAbody F(ab')₂ staining) with \pm SD error bars shown. Groups are color coded to match across the different graphics.

CAR-T cell doses across the study and persisted through day 21 when it was detected at approximately 600 ng/mL (3.2 nM) (Fig. 5d) corresponding to high levels of armed peripheral CAR cells (Fig. 5e). By day 45 of the study, the cohort receiving 35M + Rit-S3 maintained relatively high CD3⁺ T cell numbers but were not well-armed with MicAbody while the 7M + Rit-S3 cohort did have cells that maintained surface-associated MicAbody. This suggested that as MicAbody levels fell below detectable limits in the plasma, CAR arming could not be maintained at high CAR-T cell levels. An alternative possibility is that the higher CD3⁺ cell numbers in the 35M + Rit-S3 cohort reflect expansion of a graft-vs-tumor subset of cells that do not express the CAR construct. However, the elevated CD3⁺ cell numbers were not seen in the 35M pre-armed cohort suggesting that this is not the case. In summary, pre-armed *convertible*CAR-Ts were able to exert a potent anti-tumor response that inhibited tumor expansion. Furthermore, *convertible*CAR-Ts were able to effectively control a solid lymphoma when an adequate *in vivo* level of *convertible*CAR-T cell arming was maintained.

Selective delivery of biomolecules to *convertible*CAR-T cells.

The privileged interaction between iNKG2D variants and their orthogonal ligands enables the selective delivery of agents to iNKG2D-CAR expressing cells simply by fusing them as payloads to the orthogonal ligands themselves. To demonstrate the utility of this feature two disparate applications were explored: targeted ablation utilizing the complement system and selective delivery of activating cytokines. In the first application, the U2R variant was fused to either the N- or C-terminus of the wild-type human IgG1 Fc-domain or to mutant Fc domains previously described as enhancing C1q binding—S267E/H268F/S324T/G236A/I332E (“EFTAE”)²⁰ and K326A/E333A (“AA”)²¹ (Supplementary Fig. 8a). Using just the Fc-portion, as opposed to a complete therapeutic antibody targeting an epitope-tagged CAR cell, avoids collateral effects from opsonization of non-iNKG2D expressing cells^{22–24}. The enhanced C1q binding was confirmed by ELISA with relative order of Kd’s as EFTAE < AA < wt (Supplementary Fig. 8g). While iNKG2D.AF-CAR cells were susceptible to killing by human complement in a manner that was dependent upon both concentration and C1q affinity (Supplementary Fig. 8c), untransduced cells were unaffected. Interestingly, orientation of the U2R fusion was critical - N-terminal fusions, which orient the Fc in a manner consistent with an antibody were much more effective. Similar results were obtained with the U2S3 and iNKG2D.YA pairing (Supplementary Fig. 8d).

The potential ability of orthogonal ligands to deliver cytokines selectively to iNKG2D-CAR expressing cells has advantages to not only promote their expansion but also potentially leverage differential cytokine signaling to control T cell phenotype and function. As a general design principle, mutant cytokines with reduced binding to their natural receptor complexes were employed to reduce their engagement with immune cells not expressing the CAR and to minimize toxicity associated with wild-type cytokines. Additionally, cytokine fusions were kept monovalent to eliminate avidity-enhanced binding and signaling. To this end, the R38A/F42K mutations in IL-2 (mutIL2)²⁵ and the V49D mutation in IL-15 (mutIL15)²⁶ dramatically reduce binding to each cytokine’s respective Ra subunit while maintaining IL-2Rβ/γ complex engagement. Initial experiments using the iNKG2D.YA orthogonal variant U2S2 fused to either mutIL2 or mutIL15 promoted proliferation of iNKG2D.YA-CAR expressing cells but not those expressing wtNKG2D-CAR (Supplementary Fig. 9a). Both cell populations expanded in the presence of the ULBP2.R81W variant, which does not discriminate between wtNKG2D and iNKG2D.YA. Direct fusion to the ligand or via a heterodimeric Fc linkage²⁷ (e.g., U2S2-hFc-mutIL2) promoted

expansion of GFP⁺ *convertible*CAR-T cells to densities above the untransduced cells present (Supplementary Fig. 9b), and these expanded *convertible*CAR-T cells maintained their cytolitic capabilities (Supplementary Fig. 9c). Engagement of iNKG2D.YA by MicAbody, monovalent U2S3-hFc (without a cytokine payload), or by mutIL2 alone were insufficient to drive proliferation of *convertible*CAR-CD8⁺ cells (Supplementary Fig. 9a, d). Flow cytometry characterization of STAT3 and STAT5 phosphorylation (pSTAT3 and pSTAT5) revealed that exposure to wild-type IL-2 or IL-15 resulted in an increase of pSTAT3 and pSTAT5 in both untransduced as well as *convertible*CAR-CD8⁺ cells (Supplementary Fig. 9e). Treatment of untransduced cells with U2S3-hFc-mutIL2 resulted only in a minimal shift in pSTAT5 relative to the no cytokine control, consistent with mutIL2’s retention of IL-2Rβ/γ binding. The *convertible*CAR-CD8⁺ cells responded to both U2S3-hFc-mutIL2 and U2S3-hFc-mutIL15 with an increase in pSTAT5 levels via γ-chain activation of JAK3. Unlike wild-type cytokines, no increase in pSTAT3 signal was observed, indicating a reduction in JAK1 activation through IL-2Rβ²⁸ in both scenarios as a consequence of disruption of Ra binding, a hypothesis supported by IL-15Rα’s role in increasing the affinity of IL-15 for IL-2Rβ²⁹. The kinetics of responses U2S3-hFc-mutIL2 and U2S3-hFc-mutIL15 were nearly identical, indicating functional redundancy in their mutant forms (Supplementary Fig. 9f).

U2S3-hFc-mutIL2 was shown to have an *in vivo* PK half-life of a few days (Supplementary Fig. 9g). *convertible*CAR-T cells administered to NSG mice in the absence of tumor underwent a homeostatic expansion, peaking at 3 days followed by contraction. Three injections of U2S3-hFc-mutIL2 staged 1 week apart resulted in a dramatic expansion of human T cells in the peripheral blood (Fig. 6a) and T cell numbers contracted after cessation of U2S3-hFc-mutIL2 support with CD8⁺ T cells driving the bulk of the expansion. In parallel with expansion, the proportion of GFP⁺ CD8⁺ T cells increased to 100% demonstrating selective expansion of iNKG2D-CAR expressing cells but not untransduced cells (Fig. 6b).

The effect of U2S3-hFc-mutIL2 on normal human PBMCs from three donors was explored *in vitro* by exposure to increasing concentrations of the agent for 4 days followed by flow-based quantification of cells positive for the proliferative marker Ki-67 (Supplementary Fig. 10). In addition to the -mutIL2 fusion, a wild-type IL2 fusion (U2S3-hFc-wtIL2) was included to directly demonstrate that the reduction in mutIL2 bioactivity was a consequence of the mutations employed and not the fusion format itself. The CD4⁺ and CD8⁺ T cells responded robustly to both anti-CD3 and wild-type IL-2 positive controls as well as to the lowest dose of U2S3-hFc-wtIL2. Proliferative responses to U2S3-hFc-mutIL2 occurred in a dose-dependent manner with expansion observed across donors at levels above 300 IUe/mL but not achieving levels comparable to those of the IL-2 positive control until 30,000 IUe/mL. Treg responses were comparable to those of CD4⁺ and CD8⁺ cells with the exception of cells from one donor (who additionally had a muted response to anti-CD3 stimulation) that responded to U2S3-hFc-mutIL2 at a lower concentration than the other donors. Taken together, these data support the hypothesis that normal human PBMCs do not respond to U2S3-hFc-mutIL2 except at super-physiologic levels which potentially provides a wide dosing window for selective delivery of ligand-fused mutIL2 to *convertible*CAR cells while minimizing toxicity and Treg activation.

Discussion

We have described the engineering of a privileged receptor-ligand (iNKG2D.YA and U2S3) pairing comprising human components

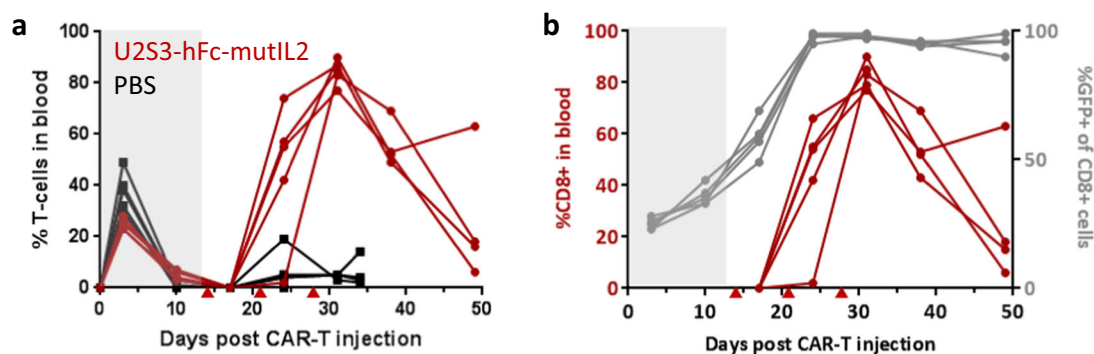


Fig. 6 In vivo response of convertibleCAR-T cells to U2S3-hFc-mutIL2. **a** NSG mice were injected with 7×10^6 total iNKG2D-transduced cells (CD4:CD8 1:1). After the contraction of T cells at 14 days, mice were injected with $30 \mu\text{g}$ U2S3-hFc-mutIL2 or PBS once per week—indicated by red triangles—and T cell dynamics monitored by flow cytometry. Shown are the % of human CD3⁺ T cells in the peripheral blood with each trace corresponding to an individual mouse, $n = 5$. **b** Plots for the expansion of CD8⁺ cells as well as the increase in proportion of GFP⁺ (CAR-expressing) cells upon U2S3-mutIL2 treatment.

for a highly adaptable CAR, resulting in a versatile and broadly controllable platform. The iNKG2D.YA-CAR receptor itself is held invariant on T cells with CAR function readily directed to potentially any antigen of interest by virtue of attaching the orthogonal ligand to the appropriate antigen-recognizing antibody. In this manner, the same convertibleCAR-T cells can be retargeted as needed if, for example, the original tumor antigen becomes downregulated during the course of therapy. This targeting flexibility is not limited to the sequential engagement of antigens, but can also be multiplexed to simultaneously direct T cells to more than one antigen in order to reduce the likelihood of tumor escape by antigen loss, address the issue of heterogeneity of intratumoral antigen expression, or even simultaneously target tumor and suppressive cellular components of the tumor microenvironment. Traditional scFv-CAR cells are generally committed to a fixed expression level of a receptor which reduces their ability to discriminate between antigen levels present on healthy versus aberrant cells. The use of switch/adaptor strategies, like MicAbodies with convertibleCAR-T cells, may provide an opportunity to differentially engage CAR-Ts to achieve a therapeutic index that reduces the risk of severe adverse events³⁰. While all adaptor strategies require the initial development of two components, once the CAR architecture has been established each iterative round of adaptor development will involve relatively minor modifications to the original antibody-based adaptor without alterations to the manufacturing process.

The use of the privileged receptor-ligand interaction for delivery of payloads specifically to iNKG2D-bearing cells without additional cellular engineering is another advantage. The capability of harnessing interleukin functions to drive expansion and activation, prevent exhaustion, or even promote suppression in a controlled and targeted manner could have beneficial consequences for efficacy and safety. Introduction of cytokine-ligand fusions during CAR manufacturing could address qualitative and quantitative limitations of patient T cells and their administration post-CAR infusion could expand the number of CAR-T cells and their persistence which, with CD19-CAR therapies, is correlated positively with response rates³¹. Most CAR therapies require a preconditioning lymphodepletion regimen to promote engraftment and expansion of CAR cells, one rationale being that it provides a more verdant immunological setting for CARs to expand³². Robust and controllable convertibleCAR-T expansion in patients may supplant the need for lymphodepletion, allowing for retention of endogenous immune functions that are fully competent to support the initial convertibleCAR-mediated anti-tumor activity. Another clinical strategy might be to deliver

cytokine-ligand fusions to bolster convertibleCAR-T function, possibly with a cycling regimen to reduce T cell exhaustion and promote the maintenance of memory T cells³³. And lastly, as CARs have been demonstrated to persist in humans for years post-infusion³⁴, the ability to recall resident convertibleCAR-Ts to attack primary or secondary malignancies (either with the original targeting MicAbody or a different one) without having to re-engineer or generate a new batch of CAR cells should be highly advantageous. Unlike scenarios where CARs have been engineered to constitutively express cytokines^{35,36}, delivery of cytokines exclusively to convertibleCAR-T cells can be modulated depending upon the manufacturing or clinical needs.

By design, each component of the convertibleCAR system—the iNKG2D-based CAR receptor and the MicAbody (which is ADCC-deficient)—are functionally inert on their own. This has advantages during manufacturing, particularly in the context of indications such as T cell malignancies where traditional scFv-based CARs encounter expansion hurdles due to fratricide³⁷. Additionally, it provides enhanced control of CAR function during treatment. We have demonstrated that convertibleCAR-T cells can be armed with MicAbody prior to administration to provide an initial burst of anti-tumor activity on par with traditional scFv-CARs, an aspect that will be critical for first-in-human safety studies. In addition to activation-induced replication, these cells also internalize their engaged CAR receptors in a manner consistent with what has been observed with other 4-1BB/CD3 ζ scFv-CARs³⁸ (Supplementary Fig. 5c). As a consequence of these two processes, convertibleCAR-T cells will rapidly disarm after initial expansion and target engagement, which then provides an opportunity to rearm and re-engage in a manner controlled by MicAbody dosing.

In addition to the iNKG2D-U2S3 pairing based upon ULBP2, we have also identified high-affinity orthogonal MicA and ULBP3 variants to iNKG2D.YA that are non-redundant in their amino acid compositions through the helix 4 domain. The fact that a convergence of sequence was not observed, despite the conserved tertiary structure of their MIC $\alpha_1\alpha_2$ domains, indicates that there are many solutions for orthogonality. Additionally, we have engineered a completely independent iNKG2D.AF and U2R pairing suggesting that there is opportunity to explore a breadth of inert NKG2D variants that, in combination with mutational space afforded by the MIC ligands, can lead to the identification of additional orthogonal receptor-ligand pairings. Having mutually exclusive receptor-ligand pairs would enable, for example, their introduction into distinct cell populations (e.g., CD4 and CD8 T cells) to differentially engage them as needed.

Furthermore, within the same cell, the two iNKG2D variants could be expressed with split intracellular signaling domains to provide dual antigen-dependent activation to enhance on-tumor selectivity^{39,40}. Alternatively, the two iNKG2D variants could be differentially linked to either activating or immunosuppressive domains to enhance the discriminatory power of the T cells between tumors or healthy tissue, respectively⁴¹.

In summary, the *convertible*CAR system has demonstrated capabilities to not only be readily targeted to different cell-surface antigens but can also be selectively engaged exogenously to drive cell expansion. The privileged receptor-ligand interaction that has been developed is agnostic to cell type and can, in principle, be engineered into any cell of interest as long as the cell-appropriate signaling domains are provided. Additionally, the adoptive cellular therapy field is aggressively pursuing the development of allogeneic cells to bring down the time, complexity, and cost of manufacturing to provide a more consistent, readily accessible product^{31,42}. A highly adaptable CAR system would be powerfully synergistic with allogeneic efforts and once a truly universal allogeneic CAR system has been validated, the therapeutic field then becomes characterized by the relative ease of developing and implementing a library of adapter molecules from which personalized selections can be made. This strategy also broadens the potential areas of application to any pathogenic cell with a targetable surface antigen. For example, we have recently demonstrated the utility of *convertible*CAR platform in the *ex vivo* reduction of latent reservoirs in the blood of HIV patients using a cocktail of MicAbodies derived from anti-HIV broadly neutralizing antibodies⁴³.

Methods

Cloning, expression, and purification. The wild-type ectodomain of NKG2D (UniProtKB P26718, residues 78–216; <https://www.uniprot.org>) was expressed as a fusion to the C-terminus of human IgG1 Fc via a short factor Xa recognizable Ile-Glu-Gly-Arg linker (Fc-wtNKG2D). Inert NKG2D variants comprising either a single Y152A (iNKG2D.YA) or double Y152A/Y199A substitution (iNKG2D.AF)¹⁷ were generated by PCR-mediated mutagenesis or synthesized (gBlocks[®], IDT). DNA constructs for Fc-NKG2D molecules were expressed in Expi293[™] cells (Thermo Fisher Scientific) and dimeric secreted protein was purified by Protein A affinity chromatography (Pierce[™] #20334, Thermo Fisher). Eluted material was characterized and further purified by size-exclusion chromatography (SEC) on an ÄKTA Pure system using Superdex 200 columns (GE Life Sciences). Correctly assembled, size-appropriate monomeric material was fractionated into phosphate-buffered saline (PBS).

The $\alpha_1\alpha_2$ domains of human MICA*001 (UniProtKB Q29983, residues 24–205), MICB (UniProtKB Q29980.1, 24–205), ULBP1 (UniProtKB Q9BZM6, 29–212), ULBP2 (UniProtKB Q9BZM5, 29–212), ULBP3 (UniProtKB Q9BZM4, 30–212), ULBP5 (NCBI accession NP_001001788.2, 29–212), ULBP6 (UniProtKB, 29–212) were cloned with a C-terminal 6x-His tag. Monomeric protein was purified from Expi293[™] supernatants Ni-NTA resin (HisPur[™], Thermo Fisher) and eluted material exchanged into PBS with Sephadex G-25 in PD-10 Desalting Columns (GE Life Sciences).

MIC ligands and orthogonal variants were cloned by ligation-independent assembly (HiFi DNA Assembly Master Mix, NEB #E2621) as fusions to the C-terminus of either the kappa light-chain or the heavy-chain of human IgG1 antibodies via either an APTSSSGGGGS or GGGG linker, respectively. Additionally, D265A/N297A (Kabat numbering) mutations were introduced into the CH2 domain of the heavy chain of all antibody and MicAbody clones to eliminate antibody-dependent cell cytotoxicity (ADCC) function⁴⁴. Heavy- and light-chain plasmid DNAs (in the mammalian expression vector pD2610-V12 (ATUM) for a given antibody clone were co-transfected into Expi293[™] cells and purified by Protein A. For any monoclonal antibody fusion generated, the appropriate VL or VH domains were swapped into either the kappa light-chain or ADCC-deficient IgG1 heavy-chain.

Inert NKG2D and orthogonal ligand engineering. Bio-layer interferometry (BLI) with the FortéBio Octet system (Pall FortéBio LLC) was implemented to validate loss of wild-type MIC ligand binding by iNKG2D. Fc-wtNKG2D, Fc-iNKG2D.YA, or Fc-iNKG2D.AF was captured on anti-human IgG Fc capture (AHC) biosensor tips and association/dissociation kinetics monitored in a titration series of monomeric MIC-His ligands. Additionally, ELISA (enzyme-linked immunosorbent assay) binding assays were performed with MICA-Fc, MICB-Fc, ULBP1-Fc, ULBP2-Fc, ULBP3-Fc, or ULBP4-Fc (R&D Systems) coated onto microtiter plates,

a titration of biotinylated Fc-wtNKG2D or Fc-iNKG2D.YA, detected with streptavidin-HRP (R&D Systems #DY998), and developed with 1-Step Ultra TMB ELISA (Thermo Fisher #34208).

Phage display was employed to identify orthogonal ULBP2 $\alpha_1\alpha_2$ variants that exhibited exclusive binding to either iNKG2D.YA or iNKG2D.AF. Synthetic NNK (where N = A/C/G/T and K = G/T, resulting in representation of all 20 amino acids without stop codons) DNA libraries were generated targeting the codons of helix 2 (residues 74–78, numbering based upon mature protein) or helix 4 (residues 156–160) that in the bound state are positioned in close proximity to the Y152 positions on the natural NKG2D receptor⁴⁵. Libraries exploring helix 2 alone, helix 4 alone, or the combination were cloned as fusions to the pIII minor coat protein of M13 phage, and phage particles displaying the mutagenized $\alpha_1\alpha_2$ domain variants were produced in SS320 *E. coli* cells according to standard methods^{46,47}. These $\alpha_1\alpha_2$ phage libraries were captured with either biotinylated Fc-iNKG2D.YA or Fc-iNKG2D.AF protein (EZ-Link[™] NHS-Biotin Kit, Thermo Fisher #20217) and enriched by cycling through four rounds of selection with increasing concentrations of non-biotinylated Fc-wtNKG2D competitor. Positive phage clones were verified for preferential binding to plate-bound Fc-iNKG2D.YA or Fc-iNKG2D.AF versus Fc-wtNKG2D by spot ELISA and bound phage detected with biotinylated M13 phage coat protein monoclonal antibody E1 (Thermo Fisher # MA1-34468) followed by incubation with streptavidin-HRP.

Phage variants were sequenced then cloned as human IgG1 monoclonal antibody fusions (see above) for additional validation. To confirm that selectivity of orthogonal variants was maintained in the bivalent MicAbody format, ELISAs wells were coated with 1 μ g/mL Fc-wtNKG2D, Fc-iNKG2D.YA, or Fc-iNKG2D.AF and bound MicAbody detected with an HRP-conjugated mouse-anti-human kappa chain antibody (Abcam #ab79115). Affinity of both monomeric and antibody-fused ULBP2 variants was also determined by Octet analysis as described above.

Generation of convertibleCAR-T cells. Human-codon optimized DNA (GeneArt, Thermo Fisher) comprising the CD8 α -chain signal sequence, NKG2D variant, CD8 α hinge, and transmembrane domains, 4-1BB, CD3 ζ , and eGFP were cloned into the pHR-PGK transfer plasmid for second generation Pantropic VSV-G pseudotyped lentivirus production along with packaging plasmids pCMV Δ R8.91 and pMD2.G⁴⁸. The VH and VL domains of rituximab separated by a (GGGS)₃ linker were substituted for the NKG2D module to generate the rituximab scFv-based CAR (RITscFv-CAR). For each batch of lentivirus produced, 6 \times 10⁶ Lenti-X 293T (Takara Bio #632180) cells were seeded in a 10 cm dish the day prior to transfection. Then 12.9 μ g pCMV Δ R8.91, 2.5 μ g pMD2.G and 7.2 μ g of the pHR-PGK-CAR constructs were combined in 720 μ l Opti-MEM[™] (Thermo Fisher #31985062) then mixed with 67.5 μ l of Fugene HD (Promega Corp. E2311), briefly vortexed, and incubated at room temperature for 10 min before adding to the dish of cells. After 2 days, supernatants were collected by centrifugation and passed through 0.22 μ m filters. 5X concentrated PEG-6000 and NaCl were added to achieve final concentrations of 8.5% PEG-6000 (Hampton Research #HR2-533) and 0.3 M NaCl, incubated on ice for two hours, then centrifuged at 4 $^{\circ}$ C for 20 min. Concentrated viral particles were resuspended in 0.01 volume of PBS, and stored frozen at –80 $^{\circ}$ C.

For primary human T cell isolation, a Human Peripheral Blood Leuko Pak (Stemcell Technologies #70500.1) from an anonymous donor was diluted with an equivalent volume of PBS + 2% FBS, then centrifuged at 500 \times g for 10 min at room temperature. Cells were resuspended at 5 \times 10⁷ cells/ml in PBS + 2% FBS and CD4⁺ or CD8⁺ cells enriched by negative selection (Stemcell EasySep[™] Human CD4 T Cell Isolation Kit #17952 or EasySep Human CD8 T Cell Isolation Kit #17953) by addition of 50 μ l of isolation cocktail per ml of cells and incubating for 5 min at room temperature. Subsequently, 50 μ l of RapidSpheres[™] were added per ml of cells and samples topped off (to each 21 mL cells, 14 mL of PBS). Cells were isolated for 10 min with an EasySEP[™] magnet followed by removal of buffer while maintaining the magnetic field. Enriched cells were transferred into new tubes with fresh buffer and the magnet reapplied for a second round of enrichment after which cells were resuspended, counted, and cryopreserved at 10–15 \times 10⁶ cells/cryovial (RPMI-1640, Corning #15-040-CV; 20% human AB serum, Valley Biomedical #HP1022; 10% DMSO, Alfa Aesar #42780).

To generate CAR-T cells, one vial of cryopreserved cells was thawed and added to 10 ml T cell medium “TCM” (TexMACS medium, Miltenyi 130-097-196; 5% human AB serum, Valley Biomedical #HP1022; 10 mM neutralized N-acetyl-L-cysteine; 1 \times 2-mercaptoethanol, Thermo Fisher #21985023, 1000 \times ; 45 IU/ml human IL-2 IS “rhIL-2”, Miltenyi #130-097-746). Cells were centrifuged at 400 \times g for 5 min then resuspended in 10 ml TCM and adjusted to 1 \times 10⁶/ml and plated at 1 ml/well in a 24 well plate. After an overnight rest 20 μ l of Dynabeads[™] Human T-Activator CD3/CD28 (Thermo Fisher #1131D) were added per well and incubated for 24 h. Concentrated lentiviral particles (50 μ l) were added per well, cells incubated overnight, then transferred to T25 flasks with an added 6 ml TCM. After 3 days of expansion, Dynabeads were removed (MagCelect magnet, R&D Systems MAG997), transduction efficiency assessed by flow cytometry for GFP, back-diluted to 5 \times 10⁵ cells/mL, and cell density monitored daily to ensure they did not exceed 4 \times 10⁶ cells/ml. When necessary, surface expression of iNKG2D was correlated with GFP expression using a MicAbody and detecting with PE-anti-human kappa chain (Abcam #ab79113) or by directly conjugating the Rituximab-MicAbody to Alexa Fluor 647 (Alexa Fluor Protein Labeling Kit #A20173, Thermo

Fisher). The amount of iNKG2D expression on the surface of *convertible*CAR-CD8⁺ cells was quantified using Alexa Fluor 647 conjugated Rituximab-MicAbody, and median fluorescence intensity was correlated with Quantum™ MESF 647 beads (Bangs Laboratories #647). All flow cytometry was performed on either Bio-Rad S3e Cell Sorter or Miltenyi MACSQuant Analyzer 10 instruments.

Cell lines and in vitro assays. Ramos human B cell lymphoma cells (ATCC #CRL-1596) were cultured in RPMI supplemented with 20 mM HEPES and 10% FBS. The mouse colon carcinoma line CT26 transfected to express human Her2 were a kind gift from Professor Sherie Morrison (UCLA). No additional mycoplasma testing nor authentication was performed except to verify by flow cytometry that target antigens were expressed.

For calcein-release assays, tumor cells were centrifuged and resuspend in 4 mM probenecid (MP Biomedicals #156370) + 25 μM calcein-AM (Thermo Fisher #C1430) in T cell medium at 1–2 × 10⁶ cells/ml for one hour at 37 °C, washed once, and adjusted to 8 × 10⁵ cells/ml. CD8⁺ CAR-T cells were pelleted and resuspended in 4 mM probenecid with 60 IUe/ml IL-2 in TCM at 4 × 10⁶ cells/mL then adjusted according to the desired effector:target ratio (unadjusted for transduction efficiency). 25 μL target cells were plated followed by 25 μL medium or diluted MicAbody. Then 100 μL medium (minimum lysis), medium + 3% Triton-X 100 (maximum lysis), or CAR-T cells were added and plates incubated at 37 °C for 2 h. Cells were pelleted and 75 μL supernatant transferred to black clear-bottom plates and fluorescence (excitation 485 nm, emission cutoff 495 nm, emission 530 nm, 6 flashes per read) acquired on a Spectramax M2e plate reader (Molecular Devices). For experiments with armed *convertible*CAR-CD8⁺ cells, T cells were pre-incubated at 37 °C with either saturating (5 nM) or a titration of MicAbody for 30 min before washing to remove unbound MicAbody and co-culturing with calcein-loaded target cells.

In order to quantify the target-dependent activation of T-cells, experiments were set up as described above except that calcein-preloading was omitted and assays set up in T cell medium without IL-2 supplementation. After 24 h co-culture, supernatants were harvested and stored at –80 °C until the amount of liberated cytokine could be quantified by ELISA MAX™ Human IL-2 or Human IFN-γ detection kits (BioLegend #431801 and #430101).

The MicAbody binding curve data were generated by ProMab Biotechnologies, Inc. (Richmond, CA). 3 × 10⁵ *convertible*CAR-CD8⁺ cells were plated in 96-wells V-bottom plates and incubated with labeled Alexa Fluor 647 labeled Rituximab.LC-U2S3 MicAbody for 30 min at room temperature in a final volume of 100 μL RPMI + 1% FBS with a titration curve starting at 200 nM. Cells were then rinsed and median fluorescence intensity determined for each titration point by flow cytometry.

Animal studies. All animal studies were conducted by ProMab Biotechnologies, Inc. (Richmond, CA) with the exception of the U2S3-hFc-mutIL2 pharmacokinetic (PK) sampling which was conducted by Murigenics (Vallejo, CA). For PK analysis of serum levels of MicAbodies, 6-week old female NSG mice (NOD.Cg-Prkdc^{scid}IL2rg^{tm1Wjl/Sz}, The Jackson Laboratory # 005557) were injected intravenously (IV) with 100 μg of either parent rituximab antibody (ADCC-defective), heavy-chain U2S3 fusion of rituximab (Rituximab.HC-U2S3), or light-chain fusion (Rituximab.LC-U2S3). Collected sera were subjected to ELISA by capturing with human anti-rituximab idio-type antibody (HCA186, Bio-Rad Laboratories), detected with rat-anti-rituximab-HRP antibody (MCA2260P, Bio-Rad), and serum levels interpolated using either a rituximab or Rituximab-U2S3 standard curve. PK analysis of U2S3-hFc-mutIL2 was performed in NSG mice by IP injection of 60 μg followed by regular serum collection. Samples were examined by ELISA capturing with Fc-iNKG2D and detecting with biotinylated rabbit-anti-human IL-2 polyclonal antibody (Peprotech #500-P22BT) followed by incubation with streptavidin-HRP. Half-lives were calculated in GraphPad Prism based upon the β-phase of the curve using a nonlinear regression analysis, exponential, one-phase decay analysis with the plateau constrained to zero.

For disseminated Raji B cell lymphoma studies, 6-week old female NSG mice were implanted IV with Raji cells (ATCC #CCL-86) stably transfected to constitutively express luciferase from *Luciola italica* (Perkin Elmer RediFect Red-FLuc-GFP #CLS960003). Initiation of treatment administration is detailed in each in vivo study figure. For all experiments, CD4 and CD8 primary human T cells were independently transduced, combined post-expansion at a 1:1 mixture of CD4:CD8 cells without normalizing for transfection efficiency between cell types or CAR constructs, and the mixture validated by flow cytometry prior to IV injection. Administration of MicAbody or control antibody was by the intraperitoneal (IP) route unless otherwise specified, and in vivo imaging for bioluminescence was performed with a Xenogen IVIS system (Perkin Elmer). Animals were bled regularly to monitor human T cell dynamics by flow cytometry, staining with APC Anti-Human CD3 (clone OKT3, #20-0037-T100, Tonbo Biosciences), monitoring GFP, and examining cell-associated MicAbody levels with biotinylated Anti-Human F(ab')₂ (#109-066-097, Jackson ImmunoResearch Laboratories Inc.) followed by Streptavidin-PE detection (BD #554061). Supplementary Fig. 11 provides an example of the gating strategy implemented. Serum ELISAs to monitor MicAbody levels was performed as described above.

For subcutaneous tumor studies 1 × 10⁶ Raji cells were implanted in matrigel on the right flank of 6-week old female NSG mice and therapy initiated when tumors

reached 70–100 mm³. For the cohort that received armed *convertible*CAR-T cells, the cells were incubated with 5 nM Rituximab.LC-U2S3 MicAbody ex vivo for 30 min at room temperature before washing and final mixing to achieve the desired 1:1 CD4:CD8 ratio and cell concentration. Arming was confirmed by flow cytometry with the biotinylated Anti-Human F(ab')₂ antibody and revealed a strong correlation between GFP and F(ab')₂ MFIs. These mice did not receive a separate MicAbody administration. Caliper measurements were regularly taken to estimate tumor volume (L × W × W × 0.5 = mm³), and terminal tumor masses were weighed.

This manuscript does not contain studies performed by any of the authors. All procedures involving animals were done in accordance with the ethical and regulatory standards of the institution at which the studies were conducted and performed according to protocols approved by the Institutional Animal Care and Use Committee. All applicable international, national, and/or institutional guidelines for the care and use of animals were followed.

Complement-mediated ablation of iNKG2D.AF-CAR cells. To generate Fc reagents with enhanced complement binding and targeted delivery to the T cells expressing iNKG2D.AF, the orthogonal ligand was cloned as a fusion to either the N- (U2R-Fc) or C-terminus (Fc-U2R) of human IgG1 Fc via a GGG linker with the Fc including the hinge, CH2, and CH3 domains. In addition to the wild-type Fc, the K326A/E333A²¹ (Kabat numbering, “AA”) and S267E/H268F/S324F/G236A/I332E²⁰ (“EFTAE”) C1q-enhanced binding mutation sets were explored. All were expressed in Expi293T cells, purified, and fractionated as described above. Confirmatory ELISAs were performed by capturing with Fc-iNKG2D.AF followed by binding U2R/Fc-variant fusions at 1 μg/mL concentration, titrating in human-C1q protein (Abcam #ab96363), then detecting with polyclonal sheep-anti-C1q-HRP antibody (Abcam #ab46191). Complement-dependent cytotoxicity (CDC) assays were performed by iQ Biosciences (Berkeley, CA). Briefly, 5 × 10⁴ CD8⁺ cells from an NKG2D.AF-CAR transduction were plated in 96-well plates and incubated for three hours with a serial dilution of each U2R/Fc-variant fusion, in triplicate, in the presence of normal human serum complement (Quidel Corporation) at a final concentration of 10% (v/v). Cells were then harvested and resuspended with SYTOX™ Red dead cell stain (Thermo Fisher) at a final concentration of 5 μg/mL and analyzed by flow cytometry. EC₅₀ values for cytotoxicity were calculated in GraphPad prism fitted to a non-linear regression curve.

Delivery of mutant-IL2 to T cells expressing iNKG2D-CAR. To generate a reagent that was monomeric for the U2S3 ligand, monomeric for a mutant IL-2 with the inability to bind IL-2Rα (mutIL2, R38A/F42K)^{25,49} yet retained serum stability, a heterodimeric Fc strategy was employed²⁷. U2S3 was fused to the N-terminus of the Fc-hinge of one chain with K392D/K409D (Kabat numbering) mutations while the mutIL2 was fused to the C-terminus of the second Fc-chain which harbored E356K/D399K mutations. Additionally, D265A/N297A mutations were introduced in both Fc chains to render the Fc ADCC-deficient. Expression in Expi293T cells and purification was as described above. Appropriately assembled U2S3-hFc-mutIL2 material was fractionated by SEC and the presence of individual size-appropriate polypeptides was confirmed by denaturing SDS-PAGE. A direct fusion between orthogonal ligand and mutIL2 expressed as a single polypeptide with a linker comprising glycine-serine linkages, a FLAG tag, and a 6×His tag was also generated and purified by Ni-NTA exchange chromatography⁵⁰. Determination of IUe activity equivalents was based on the calculation that a 4.4 μM solution of wild-type IL-2 has the equivalent of 1000 IU/μL. IL-15 with a V49D mutation, which reduced binding to IL-15Rα but retained bioactivity²⁶, was similarly formatted with U2S3.

CAR-T cell proliferation in response to various cytokines or U2S3-cytokine fusions was quantified with the WST-1 Cell Proliferation Reagent (Millipore Sigma #5015944001). Briefly, CAR-T cells were pelleted and resuspended in T cell media without IL-2, dispensed into 96-well plates at 4 × 10⁴ cells/well, and the appropriate amount of diluted U2S3-cytokine fusions was added to achieve 30 IUe/mL or higher concentration as needed in a final assay volume of 100 μL per well. Recombinant-human IL2 and IL15 (Peprotech #200-02 and #200-15) were included as controls. After incubation for 3 days at 37 °C, 10 μL of WST-1 was added to each well and allowed to incubate for 30–60 min before quantifying intensity of color development on a plate reader. Changes in the proportion of GFP⁺ CAR-expressing cells in response to U2S3-cytokine fusion were monitored by flow cytometry. To monitor activation of STAT3 or STAT5 upon cytokine-fusion engagement cells were rested overnight in TCM media without IL-2 supplementation then treated with 150 IUe/mL IL-2, IL-15, U2S3-hFc-mutIL2, or U2S3-hFc-mutIL15 for 2 h before fixing and staining for intracellular phospho-STAT3 (Biologend PE anti-STAT3 Tyr705 clone 13A3-1) and -STAT5 (BD Alexa Fluor 647 anti-STAT5 pY694 clone 47). To monitor a temporal response, treated *convertible*CAR-CD8⁺ T cells were fixed at 0, 30, 60, and 120 min after exposure to cytokines or U2S3-hFc-cytokine fusions then stained.

Human PBMC stimulation and immune-phenotyping studies were performed by iQ Biosciences. Briefly normal PBMCs from three donors were seeded in 96-well plates at 1 × 10⁵ cells/well and exposed to a 10-fold dilution series of either U2S3-hFc-mutIL2 or U2S3-hFc-wtIL2 (wild-type IL2) for 4 days at 37 °C with 5% CO₂. Positive controls included wells coated with anti-human CD3 (OKT2) at 2 μg/mL and rhIL-2 at 300 IUe/mL. After incubation, cells were treated with TruStain FcX

block (BioLegend #422301) followed by staining with BioLegend antibody panels for proliferating T cells (CD8 clone RPA-T8 #301050, CD4 clone OKT4 #317410, CD3 clone OKT3 #300430, KI-67 #350514), and Treg cells (Fox3 clone 206D #320106, CD4 clone OKT4, CD3 clone OKT3, KI-67).

Statistics and reproducibility. All statements of reproducibility were included in the figure legends and indicate the number of experiments that the presented data were representative of. All statistical tests were performed using GraphPad Prism and analysis tools implemented are detailed in the appropriate figure legends.

Reporting summary. Further information on research design is available in the Nature Research Reporting Summary linked to this article.

Data availability

No large datasets were generated or analyzed during this study therefore sharing is not applicable. Source data supporting the graphs and charts presented in the main text are available in the Supplementary Data 1 file. All relevant data are available from the authors upon reasonable request.

Received: 27 February 2020; Accepted: 20 May 2020;

Published online: 09 June 2020

References

- June, C. H. & Sadelain, M. Chimeric antigen receptor therapy. *N. Engl. J. Med.* **379**, 64–73 (2018).
- Chavez, J. C. & Locke, F. L. CAR T cell therapy for B-cell lymphomas. *Best. Pract. Res. Clin. Haematol.* **31**, 135–146 (2018).
- Park, J. H. et al. Long-term follow-up of CD19 CAR Therapy in acute lymphoblastic leukemia. *N. Engl. J. Med.* **378**, 449–459 (2018).
- Sotillo, E. et al. Convergence of acquired mutations and alternative splicing of CD19 enables resistance to CART-19 immunotherapy. *Cancer Disco.* **5**, 1282–1295 (2015).
- Turtle, C. J. et al. CD19 CAR-T cells of defined CD4⁺:CD8⁺ composition in adult B cell ALL patients. *J. Clin. Invest.* **126**, 2123–2138 (2016).
- Minutolo, N. G., Hollander, E. E. & Powell, D. J. The emergence of universal immune receptor T cell therapy for cancer. *Front. Oncol.* **9**, 176 (2019).
- Lanier, L. L. NK cell receptors. *Annu. Rev. Immunol.* **16**, 359–393 (1998).
- Houchins, J. P., Yabe, T., McSherry, C. & Bach, F. H. DNA sequence analysis of NKG2, a family of related cDNA clones encoding type II integral membrane proteins on human natural killer cells. *J. Exp. Med.* **173**, 1017–1020 (1991).
- Bauer, S. et al. Activation of NK cells and T cells by NKG2D, a receptor for stress-inducible MICA. *Science* **285**, 727–729 (1999).
- Groh, V. et al. Cell stress-regulated human major histocompatibility complex class I gene expressed in gastrointestinal epithelium. *Proc. Natl Acad. Sci. USA* **93**, 12445–12450 (1996).
- Zwirner, N. W., Dole, K. & Stastny, P. Differential surface expression of MICA by endothelial cells, fibroblasts, keratinocytes, and monocytes. *Hum. Immunol.* **60**, 323–330 (1999).
- Spies, T. Regulation of NKG2D ligands: a purposeful but delicate affair. *Nat. Immunol.* **9**, 1013–1015 (2008).
- Li, P. et al. Complex structure of the activating immunoreceptor NKG2D and its MHC class I-like ligand MICA. *Nat. Immunol.* **2**, 443–451 (2001).
- Radaev, S., Rostro, B., Brooks, A. G., Colonna, M. & Sun, P. D. Conformational plasticity revealed by the cocrystal structure of NKG2D and its class I MHC-like ligand ULBP3. *Immunity* **15**, 1039–1049 (2001).
- Zuo, J. et al. A disease-linked ULBP6 polymorphism inhibits NKG2D-mediated target cell killing by enhancing the stability of NKG2D ligand binding. *Sci Signal* **10**, eaai8904 (2017).
- McFarland, B. J. & Strong, R. K. Thermodynamic analysis of degenerate recognition by the NKG2D immunoreceptor: not induced fit but rigid adaptation. *Immunity* **19**, 803–812 (2003).
- Culpepper, D. J., Maddox, M. K., Caldwell, A. B. & McFarland, B. J. Systematic mutation and thermodynamic analysis of central tyrosine pairs in polyspecific NKG2D receptor interactions. *Mol. Immunol.* **48**, 516–523 (2011).
- Fernández-Messina, L., Reyburn, H. T. & Valés-Gómez, M. Human NKG2D-ligands: cell biology strategies to ensure immune recognition. *Front Immunol.* **3**, 299 (2012).
- Davenport, A. J. et al. Chimeric antigen receptor T cells form nonclassical and potent immune synapses driving rapid cytotoxicity. *Proc. Natl Acad. Sci. USA* **115**, E2068–E2076 (2018).
- Moore, G. L., Chen, H., Karki, S. & Lazar, G. A. Engineered Fc variant antibodies with enhanced ability to recruit complement and mediate effector functions. *MAbs* **2**, 181–189 (2010).
- Idusogie, E. E. et al. Engineered antibodies with increased activity to recruit complement. *J. Immunol.* **166**, 2571–2575 (2001).
- Paszkiwicz, P. J. et al. Targeted antibody-mediated depletion of murine CD19 CAR T cells permanently reverses B cell aplasia. *J. Clin. Invest.* **126**, 4262–4272 (2016).
- Philip, B. et al. A highly compact epitope-based marker/suicide gene for easier and safer T-cell therapy. *Blood* **124**, 1277–1287 (2014).
- Wang, X. et al. A transgene-encoded cell surface polypeptide for selection, in vivo tracking, and ablation of engineered cells. *Blood* **118**, 1255–1263 (2011).
- Heaton, K. M., Ju, G. & Grimm, E. A. Human interleukin 2 analogues that preferentially bind the intermediate-affinity interleukin 2 receptor lead to reduced secondary cytokine secretion: implications for the use of these interleukin 2 analogues in cancer immunotherapy. *Cancer Res.* **53**, 2597–2602 (1993).
- Bernard, J. et al. Identification of an interleukin-15 α receptor-binding site on human interleukin-15. *J. Biol. Chem.* **279**, 24313–24322 (2004).
- Gunasekaran, K. et al. Enhancing antibody Fc heterodimer formation through electrostatic steering effects: applications to bispecific molecules and monovalent IgG. *J. Biol. Chem.* **285**, 19637–19646 (2010).
- Miyazaki, T. et al. Functional activation of Jak1 and Jak3 by selective association with IL-2 receptor subunits. *Science* **266**, 1045–1047 (1994).
- Ring, A. M. et al. Mechanistic and structural insight into the functional dichotomy between IL-2 and IL-15. *Nat. Immunol.* **13**, 1187–1195 (2012).
- Raj, D. et al. Switchable CAR-T cells mediate remission in metastatic pancreatic ductal adenocarcinoma. *Gut*, **68**, 1052–1064, <https://gut.bmj.com/content/68/6/1052.long> (2019).
- Fraietta, J. A. et al. Determinants of response and resistance to CD19 chimeric antigen receptor (CAR) T cell therapy of chronic lymphocytic leukemia. *Nat. Med.* **24**, 563–571 (2018).
- Hay, K. A. & Turtle, C. J. Chimeric Antigen Receptor (CAR) T cells: Lessons Learned from Targeting of CD19 in B cell malignancies. *Drugs* **77**, 237–245 (2017).
- Viaud, S. et al. Switchable control over in vivo CAR T expansion, B cell depletion, and induction of memory. *Proc. Natl Acad. Sci. USA* **115**, E10898–E10906 (2018).
- Porter, D. L. et al. Chimeric antigen receptor T cells persist and induce sustained remissions in relapsed refractory chronic lymphocytic leukemia. *Sci. Transl. Med.* **7**, 303ra139 (2015).
- Hurton, L. V. et al. Tethered IL-15 augments antitumor activity and promotes a stem-cell memory subset in tumor-specific T cells. *Proc. Natl Acad. Sci. USA* **113**, E7788–E7797 (2016).
- Avanzi, M. P. et al. IL-18 Secreting CAR T cells enhance cell persistence, induce prolonged B cell aplasia and eradicate CD19⁺ tumor cells without need for prior conditioning. *Blood* **128**, 816–816 (2016).
- Scherer, L. D., Brenner, M. K. & Mamonkin, M. Chimeric antigen receptors for T-cell malignancies. *Front. Oncol.* **9**, 126 (2019).
- Walker, A. J. et al. Tumor antigen and receptor densities regulate efficacy of a chimeric antigen receptor targeting anaplastic lymphoma kinase. *Mol. Ther.* **25**, 2189–2201 (2017).
- Lanitis, E. et al. Chimeric antigen receptor T Cells with dissociated signaling domains exhibit focused antitumor activity with reduced potential for toxicity in vivo. *Cancer Immunol. Res.* **1**, 43–53 (2013).
- Kloss, C. C., Condomines, M., Cartellieri, M., Bachmann, M. & Sadelain, M. Combinatorial antigen recognition with balanced signaling promotes selective tumor eradication by engineered T cells. *Nat. Biotechnol.* **31**, 71–75 (2013).
- Fedorov, V. D., Themeli, M. & Sadelain, M. PD-1- and CTLA-4-based inhibitory chimeric antigen receptors (iCARs) divert off-target immunotherapy responses. *Sci. Transl. Med.* **5**, 215ra172 (2013).
- Torikai, H. & Cooper, L. J. Translational implications for off-the-shelf immune cells expressing chimeric antigen receptors. *Mol. Ther.* **24**, 1178–1186 (2016).
- Herzig, E. et al. Attacking latent HIV with convertible CAR-T cells, a highly adaptable killing platform. *Cell* **179**, 880–894.e10 (2019).
- Shields, R. L. et al. High resolution mapping of the binding site on human IgG1 for Fc gamma RI, Fc gamma RII, Fc gamma RIII, and FcRn and design of IgG1 variants with improved binding to the Fc gamma R. *J. Biol. Chem.* **276**, 6591–6604 (2001).
- Müller, S., Zocher, G., Steinle, A. & Stehle, T. Structure of the HCMV UL16-MICB complex elucidates select binding of a viral immunoevasin to diverse NKG2D ligands. *PLoS Pathog.* **6**, e1000723 (2010).
- Tonikian, R., Zhang, Y., Boone, C. & Sidhu, S. S. Identifying specificity profiles for peptide recognition modules from phage-displayed peptide libraries. *Nat. Protoc.* **2**, 1368–1386 (2007).
- Andris-Widhopf, J., Steinberger, P., Fuller, R., Rader, C. & Barbas, C. F. Generation of human scFv antibody libraries: PCR amplification and assembly of light- and heavy-chain coding sequences. *Cold Spring Harb. Protoc.* **2011**, pdb.prot065573 (2011).
- Morsut, L. et al. Engineering customized cell sensing and response behaviors using synthetic notch receptors. *Cell* **164**, 780–791 (2016).

49. Sauvé, K. et al. Localization in human interleukin 2 of the binding site to the alpha chain (p55) of the interleukin 2 receptor. *Proc. Natl Acad. Sci. USA* **88**, 4636–4640 (1991).
50. Ghasemi, R. et al. Selective targeting of IL-2 to NKG2D bearing cells for improved immunotherapy. *Nat. Commun.* **7**, 12878 (2016).

Acknowledgements

We would like to thank the scientists and staff of ProMab Biotechnologies for their assistance in the implementation of the B cell lymphoma animal studies. In particular, Van Dang's contributions toward study design, project management, and data analysis were critical to the success of this program.

Author contributions

K.E.L., K.C.K., K.T.R., and D.W.M. conceived the experiments. K.C.K. and K.E.L. supervised the study. S.R.W. performed most of the in vitro experiments while K.C.K., K.E.L., D.G., D.S., and S.L. performed or contributed to specific experiments. K.C.K. wrote the paper with editorial contributions provided by D.W.M., K.E.L., and K.T.R. All authors have read and approved the final submitted paper.

Competing interests

K.C.K., S.R.W., D.G., and D.W.M. declare no competing financial interests but are employees of Xyphos Biosciences, an Astellas Company. K.E.L., D.S., S.L., and K.T.L. declare no competing financial or non-financial interests. Aspects of the *convertibleCAR* platform are claimed in U.S. Patent No. 10,259,858.

Additional information

Supplementary information is available for this paper at <https://doi.org/10.1038/s42003-020-1021-2>.

Correspondence and requests for materials should be addressed to K.C.K.

Reprints and permission information is available at <http://www.nature.com/reprints>

Publisher's note Springer Nature remains neutral with regard to jurisdictional claims in published maps and institutional affiliations.



Open Access This article is licensed under a Creative Commons Attribution 4.0 International License, which permits use, sharing, adaptation, distribution and reproduction in any medium or format, as long as you give appropriate credit to the original author(s) and the source, provide a link to the Creative Commons license, and indicate if changes were made. The images or other third party material in this article are included in the article's Creative Commons license, unless indicated otherwise in a credit line to the material. If material is not included in the article's Creative Commons license and your intended use is not permitted by statutory regulation or exceeds the permitted use, you will need to obtain permission directly from the copyright holder. To view a copy of this license, visit <http://creativecommons.org/licenses/by/4.0/>.

© The Author(s) 2020